

Testing Millisecond Pulsars as the Source of the Galactic Center Excess Gamma-Ray emission

YI XING,¹ ZHONGXIANG WANG,^{2,1} AND FENG HUANG³

¹Key Laboratory for Research in Galaxies and Cosmology, Shanghai Astronomical Observatory, Chinese Academy of Sciences, 80 Nandan Road, Shanghai 200030, China; yixing@shao.ac.cn; wangzx20@ynu.edu.cn

²Department of Astronomy, School of Physics and Astronomy, Yunnan University, Kunming 650091, China

³Department of Astronomy, Xiamen University, Zengcuo'an West Road, Xiamen 361005, China

ABSTRACT

The Galactic Center Excess (GCE) γ -ray emission detected with the Large Area Telescope onboard the *Fermi Gamma-ray Space Telescope* has been considered as a possible sign for dark matter (DM) annihilation, but other possibilities such as the millisecond pulsar (MSP) origin have also been suggested. As a spectral fitting method, constructed based on properties of γ -ray MSPs, has been developed, we apply this method to the study of the GCE emission for the purpose of probing the MSP origin for the GCE. A number of ~ 1660 MSPs can provide a fit to the spectrum of the GCE emission upto ~ 10 GeV, but the higher energy part of the spectrum requires additional emission components. We further carry out a stacking analysis of 30–500 GeV data for relatively nearby γ -ray MSPs, and the resulting flux upper limits are still lower than those of the GCE emission. We consider the single DM annihilation channel $\tau^+\tau^-$ or channel $b\bar{b}$, or the combination of the two for comparison, and find they generally can provide better fits than MSPs. Combination of MSPs plus a DM channel are also tested, and MSPs plus the DM channel $b\bar{b}$ can always provide better fits. Comparing this combination case to the pure DM channel $b\bar{b}$, the MSP contribution is found to be marginally needed.

Keywords: Galactic center (565); Gamma-rays (637); Millisecond pulsars (1062); Dark matter (353)

1. INTRODUCTIONS

More than 80% of the matter in the Universe is dark matter (DM). While its nature is under intense investigation, one type of the most compelling candidates is the Weakly Interacting Massive Particles (WIMP; e.g., Bertone et al. 2005). These DM particles are expected to annihilate, producing γ -ray emission signals through possible channels that depend on the final states with different Standard Model particles (e.g., Funk 2015; Arcadi et al. 2018). This possibility has motivated indirect searches for the DM in the γ -ray band. The Large Area Telescope (LAT), the main instrument onboard the *Fermi Gamma-ray Space Telescope*, scans the whole sky every three hours in the energy range from tens of MeV to ~ 1 TeV (Atwood et al. 2009). The data collected with LAT well serve the purpose of performing indirect searches for DM-annihilation signals across the entire sky.

Targets for indirect searches are those regions supposed to have high DM densities. The Galactic Center (GC) is one of them, actually expected to be the brightest source at γ -rays from WIMP annihilations (e.g., Springel et al. 2008; Funk

2015). Diffuse excess γ -ray emission, possibly related to the annihilations around the GC, was first reported after one year's observations of *Fermi*-LAT (Hooper & Goodenough 2011). Since then, the detection of the so-called Galactic Center Excess (GCE) emission has been reported in quite a few studies (e.g., Abazajian & Kaplinghat 2012; Calore et al. 2015b; Daylan et al. 2016a; Ackermann et al. 2017a). The GCE is generally found to be spherically symmetric, having an extension of approximately 2 kpc from the GC, and have a spectrum peaking in the energy range of ~ 1 –3 GeV. These properties are consistent with the predictions of the DM annihilation models; more specifically, the DM particles of several tens of GeV could annihilate to pairs of such as b-quarks or τ -leptons, giving rise to a γ -ray spectrum that is able to fit the GCE emission (Hooper & Goodenough 2011; Abazajian & Kaplinghat 2012; Daylan et al. 2016a; Huang et al. 2016; Di Mauro 2021).

Alternatively, there is another possibility for the origin of the GCE often discussed. Thousands of unresolved millisecond pulsars (MSPs; e.g., Brandt & Kocsis

2015; Bartels et al. 2016; Abbate et al. 2018) could exist in the GC region, considered to be formed in dense globular clusters and deposited in the GC region due to the cluster evaporation and gravitational tidal disruption (Brandt & Kocsis 2015; Fragione et al. 2018). Thanks to *Fermi*, MSPs are known as a major class of γ -ray-emitting sources in our Galaxy (e.g., Smith et al. 2023). The γ -ray spectral shape of the GCE is similar to those of MSPs in the low-energy GeV band, and also several studies have suggested that the GCE morphology is compatible with the stellar distribution in the Galactic bulge (e.g., Macias et al. 2018; Abazajian et al. 2020), which would be similar to Galactic globular clusters that naturally contain many MSPs (e.g., Macias et al. 2018).

We have developed a method that constructs a spectral template for the γ -ray emission of a number of MSPs in a given region and successfully applied it to explaining the γ -ray emissions of the Galactic globular clusters (Wu et al. 2022; Zhang et al. 2022, 2023). In this method, characteristic properties of γ -ray spectra, the distribution of spin periods, characteristic ages, and the relation between γ -ray emission efficiencies and characteristic ages of the known γ -ray MSPs are taken into account. The method can also be applied to fitting large-scale γ -ray emission such as from the GCE or nearby galaxies. Given the possible MSP origin for the GCE, we have carried out the study by applying our method. Since it can be easily noted that γ -ray emission of MSPs generally have a cutoff at $\sim 1\text{--}2$ GeV energies (e.g., Xing & Wang 2016; Wu et al. 2022), the GCE emission contains much higher energy part and thus we have also tested to include the contributions from both the MSPs and the DM annihilations in our study.

In this paper, we report the results of the study. Below we first describe the *Fermi* LAT data and analysis for the GCE emission in Section 2. The procedures of the morphology study and the GCE spectral fitting are presented in Section 3 and Section 4, respectively. The results are discussed and summarized in Section 5.

2. FERMI LAT DATA AND ANALYSIS

2.1. Data

We selected the LAT events from the updated *Fermi* Pass 8 database. The region of interest (RoI) was defined as that with $|l| \leq 20^\circ$ and $1^\circ \leq |b| \leq 20^\circ$, where l and b are the Galactic longitude and latitude respectively. The events within $|b| = 1^\circ$ were excluded to avoid the strong emission from the Galactic disk, which would cause large flux uncertainties on the GCE. The time period of the LAT data was 15 yrs from 2008-08-04 15:43:39 (UTC) to 2023-08-22 04:06:35 (UTC). The *ULTRACLEANVETO* event class of the data was used,

which is recommended for studies of diffuse sources. Both the *Front* and *Back* event types were used. We included the events with zenith angles $\leq 90^\circ$, which prevents the Earth's limb contamination, and excluded the events with quality flags of 'bad'. These two event-selection criteria are recommended by the LAT team¹.

2.2. Source Model

2.2.1. Catalog Sources

We included all sources within 30° centered at the Galactic Center (GC) in the source model. The positions and the spectral parameters of the sources are provided in the recently updated *Fermi* LAT 14-year source catalog (4FGL-DR4; Ballet et al. 2023). There were 1037 point sources and 27 extended sources. When constructing the *Fermi* LAT source catalog, the weights were introduced in the maximum likelihood analysis (Abdollahi et al. 2020; Ballet et al. 2023). Events below 316 MeV contributed little with low weights (see Figure 22 in Abdollahi et al. 2020), especially in the region near the Galactic plane. In addition, only *Front* events were used in <316 MeV band in order to avoid the poor PSF and the contamination due to the Earth's limb (Abdollahi et al. 2020). Because of these, we only used the LAT events in 300 MeV to 500 GeV in the following analyses, so that the large uncertainties in modeling of the catalog sources and the background diffuse emission in the low energy band were avoided.

2.2.2. Large-Scale Diffuse Sources

In the γ -ray sky, the main large-scale diffuse sources include the Galactic and extragalactic diffuse emission, the *Fermi* bubbles, the Loop I, and the GCE component. The spectral model `gll_iem_v02_P6_V11_DIFFUSE.fit` was used for the Galactic diffuse emission, which was initially often adopted for the studies of diffuse γ -ray emission (e.g., Hooper & Slatyer 2013; Daylan et al. 2016b). It consists of the π^0 , the bremsstrahlung, and the inverse Compton scattering (ICS) components, and has only 1 free parameter, the normalization. The spectral file `iso_P8R3_ULTRACLEANVETO_V3_v1.txt` was used for the extragalactic diffuse emission. We adopted the flat intensity spatial templates given in Su et al. (2010) to describe the *Fermi* bubbles and Loop I. The latter has a large size with $b > 25^\circ$, which is outside of our RoI. In the analysis, we found that whether or not including this component did not significantly affect the spectral results, and thus we removed the Loop I template from our source model.

¹ <http://fermi.gsfc.nasa.gov/ssc/data/analysis/scitools/>

For the GCE emission, it was claimed in many studies (e.g., [Calore et al. 2015b](#); [Huang et al. 2016](#); [Daylan et al. 2016a](#)) that it has a spherically symmetric morphology centered at the GC, and the Navarro-Frenk-White (NFW) profile was generally used in previous studies. However, other profiles such as a generalized NFW (g-NFW) template and templates obtained from different considerations were also used, and the spectral results were found to be dependent on the chosen profiles (e.g., [Ackermann et al. 2017a](#)). In the analysis we first adopted a simple geometric spatial distribution for the GCE emission to reduce the dependence of the results on the template profiles. Considering most of the GCE emission is detected within 10° of the GC (see Figures 19 and 20 in [Ackermann et al. 2017a](#)), we set 1 uniform disk and 9 rings between 0° and 10° from the GC with a radius step of 1° ; in other words, 10 GCE components were set, with radius 0° – 1° , 1° – 2° , ..., and 9° – 10° , denoted as GCE_1 , GCE_2 , ..., and GCE_{10} respectively.

2.3. Maximum Likelihood Analysis

We performed the maximum likelihood analysis to the LAT data in the RoI using the source model set above. In the analysis, simple power laws were used to describe the γ -ray emissions of the *Fermi* bubbles and the 10 GCE components. The prefactor parameters for them were set free, and the power-law indices were fixed to 2. The normalizations of the Galactic and extragalactic diffuse components were also set as free parameters. For all the catalog sources included in the source model, the spectral parameters were fixed to the catalog values given in [Ballet et al. \(2023\)](#). Following [Calore et al. \(2015b\)](#), we introduced an energy-dependent weight map of the RoI in the likelihood analysis to minimize the impact of the point sources in our source model. The weights were defined as

$$w_{i,j} = \frac{1}{\left(\frac{\mu_{i,j}^{PSC}}{f_{PSC}\mu_{i,j}^{BG}}\right)^{\alpha_{PSC}} + 1}, \quad (1)$$

where $\mu_{i,j}^{PSC}$ and $\mu_{i,j}^{BG}$ are the expected numbers of photons from the point sources and the Galactic diffuse emission in the i^{th} energy bin and j^{th} pixel, respectively, calculated by creating model maps in different energy bins using *gtmodel* in *Fermitools*. The two scale parameters α_{PSC} and f_{PSC} were fixed to the default values of 5 and 0.1 ([Calore et al. 2015b](#)), respectively. In this way, the LAT events in the $[i, j]$ bins around brighter sources had lower weights.

The maximum likelihood analysis was performed in 25 evenly divided energy bins in logarithm from 0.3 GeV to 500 GeV. For the data points obtained for the 10 GCE components, only those with the fluxes greater than the

statistic uncertainties were kept. We noted that the systematic uncertainties dominated in the uncertainties of the GCE spectral results. The uncertainties induced by the Galactic diffuse emission templates were commonly considered in previous studies, which were generally evaluated by adopting different templates created with the *GALPROP* code (e.g., [Ackermann et al. 2012](#); [Calore et al. 2015b](#); [Zhou et al. 2015](#); [Ackermann et al. 2017a](#)). In the analysis, we evaluated the systematic uncertainties by repeating the likelihood analysis in each energy bin with the normalizations of the Galactic diffuse component artificially fixed to values $\pm 6\%$ deviating from the best-fit values. The deviations represent the local departures from the best-fit diffuse model, and they were found to be $\sim 6\%$ when analyzing source-free regions on the Galactic plane ([Abdo et al. 2009, 2010](#)).

GCE_1 (0° – 1° from the GC) is in the masked region, and for GCE_{10} , no significant detections were found nearly across the full energy range. We considered 8 successive energy bands for the morphology study in the energy range of 1–10 GeV, during which the GCE emission has smaller systematic uncertainties induced by different factors ([Ackermann et al. 2017b](#)). The obtained fluxes, rescaled for clarity, are shown in the left panel of Figure 1. We obtained the best-fit g-NFW profile when $\gamma = 1.1$ (see below Section 3 for details). We then adopted this profile for the full GCE in the likelihood analysis to extract the γ -ray spectrum using the procedures described above. The obtained spectrum for the full GCE emission is shown in the left panel of Figure 2. For the spectral data points, we kept those when the flux values are ≥ 2 times greater than their statistic uncertainties and otherwise used the derived 95% flux upper limits. There were cases when the -6% deviation from a best fit for the Galactic emission was set, the flux value turned to be > 2 times greater than the uncertainty. For these cases, we replaced the upper limits with the original flux measurements.

3. MORPHOLOGY OF THE GCE

We studied the morphology of the GCE emission based on the g-NFW profile ([Navarro et al. 1996, 1997](#)),

$$\rho(r) = \rho_0 \frac{(r/r_s)^{-\gamma}}{(1 + r/r_s)^{3-\gamma}}. \quad (2)$$

A scale radius of $r_s = 20$ kpc was adopted, and ρ_0 was selected such that the local DM density (at 8.5 kpc from the GC) is 0.4 GeV cm^{-3} ([Iocco et al. 2011](#)). We considered three profiles with γ values of 1.0, 1.1, and 1.2 respectively (see Figure 1), and fit the observed fluxes at different radii with the rescaled model fluxes (the model flux of a profile at 5.5° was set to be the observed value).

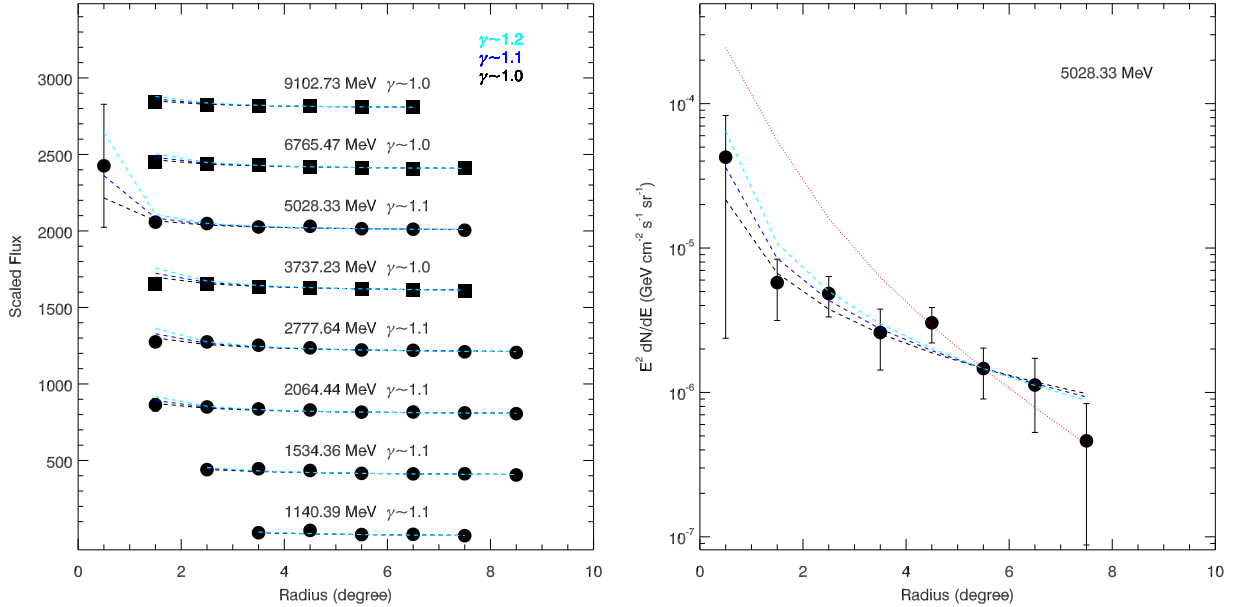


Figure 1. *Left:* rescaled γ -ray fluxes at different distances from the GC. Eight energy bands centered from 1.1 GeV to 9.1 GeV were considered. The predicted fluxes from g-NFW profiles with γ values of 1.0, 1.1, and 1.2 are plotted as dashed lines. The γ value labeled with an energy band is the best-fit one for that energy band. *Right:* γ -ray fluxes at distances of 0° – 8° from the GC at 5.0 GeV, with the g-NFW profiles plotted as dashed lines (the same as those in the left panel). The predicted profile from the stellar density distribution is plotted as a red dotted line.

χ^2 values were obtained from the fitting and the reduced χ^2 values, which are χ^2 divided by the degree of freedom (DoF), were used to determine the best fits. In our fitting, we noted that the model fluxes with $\gamma=1.2$ at 1.5° were higher than the observed ones in six out of the eight energy bands centered at ~ 2.1 – 9.1 GeV and particularly in the energy band centered at ~ 3.7 GeV, a large χ^2 value of 17.9 was obtained. Because of these, we did not further tested larger γ values in the fitting. We noted that the stellar density of the Galactic bulge given in [Vanhollebeke et al. \(2009\)](#) predicts a steeper slope than the g-NFW profile with $\gamma=1.2$. An example is shown in the right panel of Figure 1, which are the observed fluxes (without being rescaled) in the energy band centered at ~ 5.0 GeV. The predicted profile from the stellar density distribution (red dotted line) significantly deviates from the observed fluxes. Therefore this steeper profile was not considered in our analysis.

The γ values from the best-fits in each energy bands are provided in Figure 1. In three energy bands centered at ~ 3.7 , 6.8 , and 9.1 GeV (plotted as squares in Figure 1), a γ value of 1.0 was obtained with χ^2 values of 6.1, 2.7, and 0.4 (for 6, 6, and 5 DoF), and in the other five energy bands (plotted as circles in Figure 1), a γ value of 1.1 was obtained with χ^2 values of 2.0–6.3 (for 4–7 DoF). There was only one significant detection for GCE₁, which was at 5.0 GeV, and $\gamma=1.1$ was obtained in this energy band.

When we considered the g-NFW profile with a γ value of 1.1 for the energy bands centered at 3.7, 6.8, and 9.1 GeV, the χ^2 values were 9.5, 3.3, and 1.7, also acceptable for describing the emission morphology in these three bands comparing to those with a γ value of 1.0. Therefore, we adopted $\gamma=1.1$ for the g-NFW profile to describe the full GCE emission throughout the rest of the paper.

4. SPECTRAL FITTING

4.1. Millisecond pulsars

We followed the procedure given in [Wu et al. \(2022\)](#) and tested to fit the full γ -ray spectrum of the GCE emission with the spectral templates constructed for varied numbers of putative MSPs in the GC region. The γ -ray spectra of the MSPs were generated based on the spectral parameter (photon index Γ and cutoff energy E_c) ranges determined from the known γ -ray MSPs, where the distributions of their spin periods (P) and characteristic ages (τ_a), and the relation between their γ -ray efficiencies (η) and τ_a (see [Wu et al. 2022](#) for details) were considered. One difference in the fitting procedure was that we used τ_a of all known γ -ray MSPs to obtain the distribution in a form of $\log(\tau_a)$, while in [Wu et al. \(2022\)](#) because the targets were MSPs in globular clusters, the τ_a distribution of MSPs was derived by comparing with the ages of the host globular clusters. In Figure 3, we show the τ_a distribution of the known γ -ray

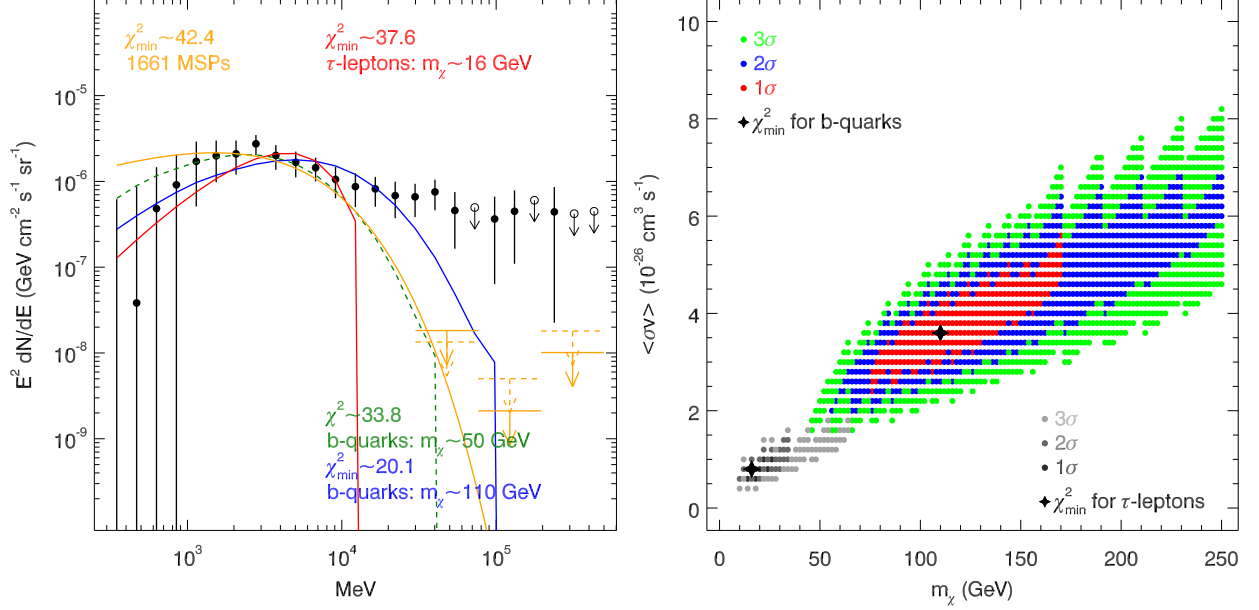


Figure 2. *Left:* γ -ray spectrum of the GCE emission. The best-fit spectra from the MSPs, and those from the DM annihilating to $b\bar{b}$ and to $\tau^+\tau^-$ are plotted as yellow, blue and red lines, respectively. The model spectrum from the DM annihilating to $b\bar{b}$ with parameters adopted from Calore et al. (2015b) is plotted as a green dashed line for comparison. The upper limits from the stacking analysis of the data of 96 and 48 γ -ray MSPs in 30–500 GeV are shown as yellow solid and dashed arrows respectively (see Section 4.1.1). *Right:* 3σ uncertainty ranges for m_χ and $\langle\sigma v\rangle$ obtained from fitting with the two annihilation channels, while the best-fit values are marked as the dark stars.

MSPs, which was fitted with a log-normal function

$$p(\tau_a) = N e^{-\frac{1}{2\sigma^2}(\log \tau_a - \mu)^2}, \quad (3)$$

where N is a normalization factor. From fitting, we obtained $\mu = 9.69$ and $\sigma = 0.42$. This function was used to generate τ_a for assumed MSPs.

We ran 1000 times of the fitting to obtain the best fit with the minimum χ^2 (χ^2_{min}) and a range for numbers of MSPs, where a source distance of 8.5 kpc was adopted and the latter was estimated from the lowest 5% χ^2_{min} values in the fitting runs. The best-fit number of MSPs was 1661 with $\chi^2_{min} = 42.4$ and the number range was 1415–1706. These results are given in Table 1.

The best-fit spectrum, emitted from 1661 MSPs, is shown in Figure 2. As can be seen, it can approximately describe the low, <10 GeV part of the spectrum of the GCE emission, but the high energy part can not be explained at all since γ -ray MSPs generally have a spectral cutoff at ~ 1 –2 GeV. In addition, the low-end of the model spectrum appears to be higher than the observed data points.

4.1.1. Stacking analysis of ≥ 30 GeV emission from millisecond pulsars

The MSP scenario for the GCE suffers different problems (e.g., Hooper & Mohlabeng 2016), and one obvious is the lack of high-energy emission from MSPs, as

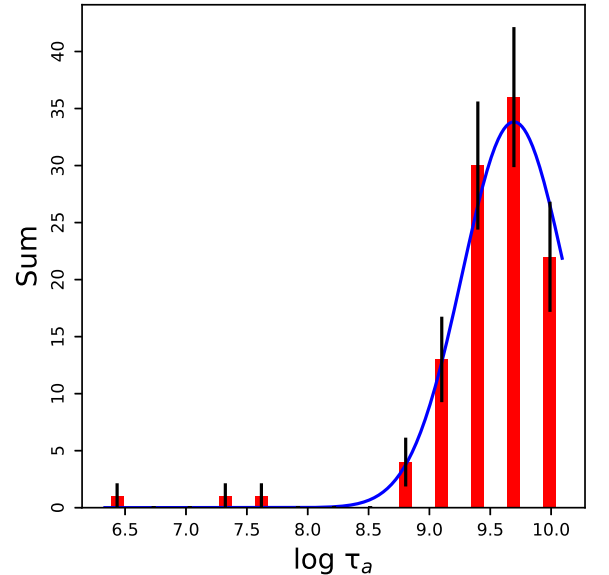


Figure 3. $\log(\tau_a)$ distribution of the known γ -ray MSPs and the corresponding best-fit log-normal function (the blue line).

shown in Figure 2. We investigated this problem with the stacking technique.

Whether pulsars have high-energy emission upto TeV energies has been probed and the very recent detection of pulsed TeV emission from the Vela

pulsar has seemingly provided encouraging results (H. E. S. S. Collaboration et al. 2023). γ -ray spectra of 104 MSPs in Wu et al. (2022) were obtained, and only one MSP, PSR J0614–3329, was noted to have significant detectable γ -ray emission in >30 GeV energy range (see Figure 2 in Wu et al. 2022). Here we applied a stacking technique to the analysis of the 30–500 GeV LAT data of γ -ray MSPs, for the purpose of finding if MSPs could have any magnetospheric emission that possibly match the high-energy part of the GCE. There are 134 γ -ray MSPs in the Galaxy listed in 4FGL-DR4, among which 115 have distance values reported in the ATNF pulsar catalog (Manchester et al. 2005). The distance distribution of them is shown in Figure 4. There are 48 MSPs within distances of 1–2 kpc and 96 MSPs within distances of 0–3 kpc. We selected the 96 MSPs with distances ≤ 3 kpc as the target sources. The same time period of the LAT data as that for the GCE was chosen, but the *SOURCE* event class of the data was used, which is recommended for studies of point sources.

We first performed the binned likelihood analysis to the 30–500 GeV LAT data within a $20^\circ \times 20^\circ$ region centered at each of the 96 MSPs. For each target MSP, a source model containing all the catalog sources within 20 deg from the MSP was used. The background Galactic and extragalactic diffuse spectral models (gll_iem_v07.fits and iso_P8R3_SOURCE_V3.v1.txt respectively) were also included in this source model. The normalizations of the catalog sources within 5 deg from the target and the two background diffuse emission models were set as free parameters. From the analysis, we again found that only PSR J0614–3329 could be significantly detected in the 30–500 GeV band, having a Test Statistic (TS) value of 46. The second high TS value was only ~ 6 , obtained for PSR J1311–3430.

We then performed the stacking analysis of the 30–500 GeV data of the 96 MSPs. The procedure of the stacking analysis, partly referring to that described in Huber et al. (2012), is as follows:

1. For each of the targets, we extracted a model count cube in 10 evenly divided energy subbands in logarithm in the interested energy band, by running *gt-model* in *Fermitools* in each of the subbands. The catalog sources included in the 4FGL-DR4 were considered in the source model, with the spectral parameters fixed at the values obtained from the above likelihood analysis.
2. We extracted the residual count cube for each of the targets by subtracting the model one from the observed one.

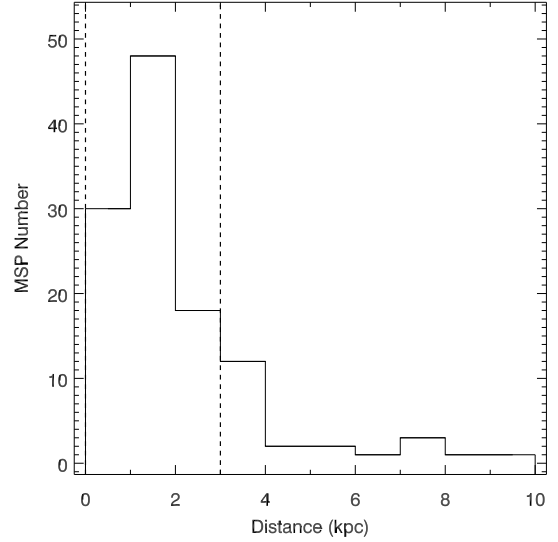


Figure 4. Distance distribution of 115 known γ -ray MSPs. The range of 0–3 kpc is marked by the dashed lines.

3. The residual count cubes for all targets were added together for the following analysis (at step 6).
4. For each of the targets, we extracted the source count cube in the 10 energy subbands with a source model including only the target source and the background Galactic and extragalactic diffuse emission. The source count cube was obtained by running *gtsrcmaps* in *Fermitools*, and the exposure cube (obtained by running *gtexposure*) was considered.
5. The source count cubes for all targets were added together as a final source count cube for the following analysis.
6. The likelihood analysis was performed to the added residual count cube with the final source count cube. The γ -ray emission from the added target was described with a power law with Γ fixed at 2. The normalizations of the target and the two background emissions were set free.

In the analysis, we repeated the stacking analysis in 3 energy bands divided in logarithm in 30–500 GeV, and derived the 95% upper limits for the added target in each of the bands. The results are given in Table 2. In the first energy band of 30.0–76.6 GeV, a TS value of 14 was obtained, corresponding to a detection significance of $>3\sigma$. This detection was likely due to emission of PSR J0614–3329 in this energy band. To compare with the GCE emission, we calculated the predicted flux upper limits for 1661 MSPs located at 8.5 kpc, assuming them within the spatial extent of the GCE. For the calculation, the added target was assumed at a distance of

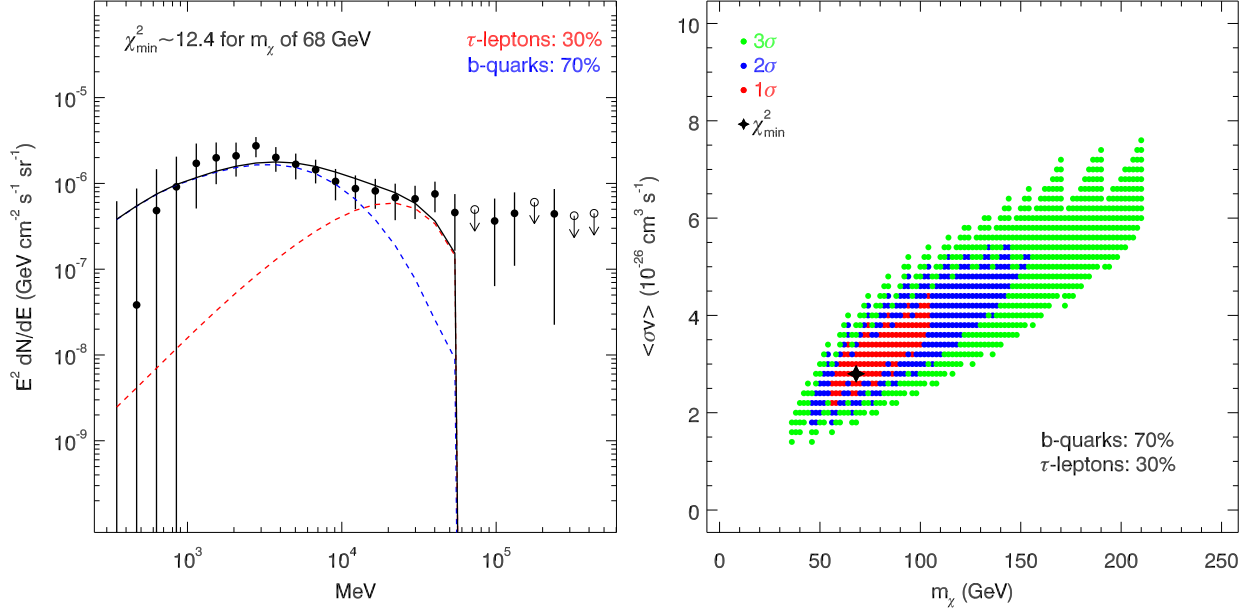


Figure 5. Fitting to the γ -ray spectrum of the GCE emission with a combination of the DM annihilating to $b\bar{b}$ and to $\tau^+\tau^-$. *Left:* the branching ratio into $b\bar{b}$ of 0.7 provides the best fit (black solid line), to which the $b\bar{b}$ and $\tau^+\tau^-$ contributions are indicated by the blue and red lines respectively. *Right:* 3σ uncertainty ranges for m_χ and $\langle\sigma v\rangle$, with the best-fit values marked as a black star.

1.5 kpc, since we only analyzed the data for the MSPs with distances of 0–3 kpc and half of them have distances of 1–2 kpc. The obtained upper limits are plotted in Figure 2 (the yellow solid arrows). As can be seen, the spectral data points of the GCE in the high energy range are higher than the upper limits.

We tested to include only the 48 γ -ray MSPs with distances of 1–2 kpc for the stacking analysis to check any possible effect due to the relatively large MSP distance range. The TS value for the added source in the first energy band (30.0–76.6 GeV) was only ~ 2 (since PSR J0614–3329 has a distance of 0.6 kpc and was not included). The obtained upper limits are shown as the dashed yellow arrows in Figure 2, still lower than the spectral data points of the GCE. We concluded that MSPs alone likely cannot explain the GCE emission.

4.2. Dark matter

In order for a comparison, we considered the DM annihilation process to fit the γ -ray spectrum of the GCE emission. The flux of the γ -ray emission generated by DM annihilations is given by

$$\phi(E_\gamma, \phi) = \frac{\langle\sigma v\rangle}{8\pi m_\chi^2} \frac{dN_\gamma}{dE_\gamma} \int_{los} \rho^2(r) dl, \quad (4)$$

where m_χ is the DM mass, $\langle\sigma v\rangle$ is the annihilation cross section, dN_γ/dE_γ is the γ -ray spectrum produced per DM annihilation, and $\rho(r)$ is the DM density as a function of distance r to the GC with the integral calculated

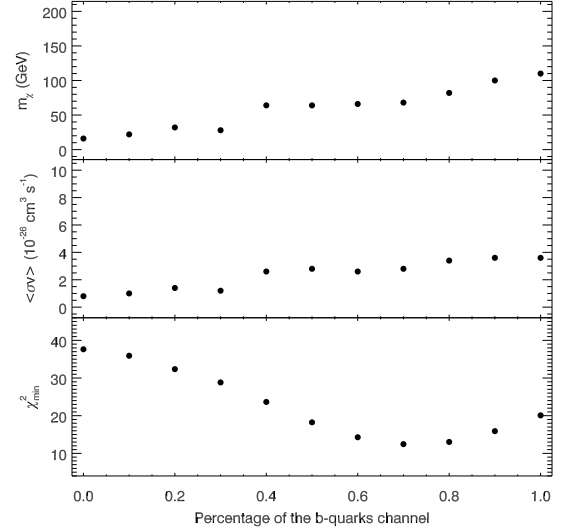


Figure 6. Obtained χ^2_{min} values as a function the branching ratio into $b\bar{b}$ (bottom panel). The corresponding $\langle\sigma v\rangle$ and m_χ values are shown in the middle and top panel respectively.

over the line-of-sight (los). In this fitting, a m_χ range of 2–250 GeV with a step of 2 GeV and a $\langle\sigma v\rangle$ range of $0.2\text{--}10 \times 10^{-26} \text{ cm}^3 \text{ s}^{-1}$ with a step of $0.2 \times 10^{-26} \text{ cm}^3 \text{ s}^{-1}$ were searched. The dN_γ/dE_γ spectra were generated using the *gammapy.astro.darkmatter* module in *Gammapy v0.20*, which is based on Cirelli et al. (2011) and provides tabulated spectral values for different annihilation channels. As the annihilation channels $\tau^+\tau^-$ and $b\bar{b}$ were commonly considered in previous studies (e.g.,

Hooper & Goodenough 2011; Abazajian & Kaplinghat 2012; Daylan et al. 2016a; Huang et al. 2016; Di Mauro 2021), we also adopted these two channels.

We found that for the channel $b\bar{b}$, a $m_\chi=110$ GeV DM with $\langle\sigma v\rangle = 3.6\times 10^{-26} \text{ cm}^3 \text{ s}^{-1}$ provides the model spectrum that relatively well fits that of the GCE emission, for which $\chi^2_{min}=20.1$. For the channel $\tau^+\tau^-$, a $m_\chi=16$ GeV DM with $\langle\sigma v\rangle = 0.8\times 10^{-26} \text{ cm}^3 \text{ s}^{-1}$ provides the best-fit spectrum among those from the channel, but with a high χ^2_{min} value of 37.6. These fitting results are given in Table 1, and the best-fit model spectra are shown in the left panel of Figure 2. In addition, the 1σ – 3σ uncertainty ranges for the two parameters are provided in the right panel of Figure 2.

A combination of the channels $b\bar{b}$ and $\tau^+\tau^-$ was tested by us, where a range of 0.0–1.0 for the branching ratio into $b\bar{b}$ was set. The best fitting was found when the branching ratio was 0.7, for which the model spectra are shown in the left panel of Figure 5. In Figure 6, the resulting χ^2_{min} values, as well as those of the DM’s m_χ and $\langle\sigma v\rangle$, are shown. The minimum χ^2_{min} was 12.4, when m_χ and $\langle\sigma v\rangle$ were 68 GeV and $2.8\times 10^{-26} \text{ cm}^3 \text{ s}^{-1}$ respectively (also given in Table 1). The 1σ – 3σ uncertainty ranges for the parameters are shown in the right panel of Figure 5.

4.3. Joint fitting

We also explored the possibility of the contributions of both MSPs and DM annihilations to the GCE. Since the lower limit for the MSP numbers estimated above was 1415, we set the MSP number from 100 to 1500 with a step of 100. Same as the above in Section 4.2, each of the annihilation channels $\tau^+\tau^-$ and $b\bar{b}$ was considered. In the fitting, we found that the channel $b\bar{b}$ often required large m_χ and $\langle\sigma v\rangle$ values when the number of MSPs was increased, and thus we considered ranges of 2–2000 GeV and 0.2 – $50\times 10^{-26} \text{ cm}^3 \text{ s}^{-1}$ (wider than above in Section 4.2) for m_χ and $\langle\sigma v\rangle$ respectively. For each-set number of MSPs, 1000 runs were conducted. The resulting 1000 spectra were averaged to obtain a single model spectrum, with the standard deviations of the former minus the latter being the uncertainties. The resulting χ^2_{min} values, as well as the DM’s m_χ and $\langle\sigma v\rangle$ values, are shown in Figure 7, with the best-fit parameter results ($\chi^2_{min} = 14.0$ and 17.1 respectively for the channels $b\bar{b}$ and $\tau^+\tau^-$) given in Table 1.

We found that the MSP plus $b\bar{b}$ model always provided better fits than the MSP plus $\tau^+\tau^-$ model (see Figure 7) for a given number of MSPs. Given that the pure DM annihilation model through the channel $b\bar{b}$ also provided better fits than that through the channel $\tau^+\tau^-$ (Section 4.2), we focused on the details of the MSP plus

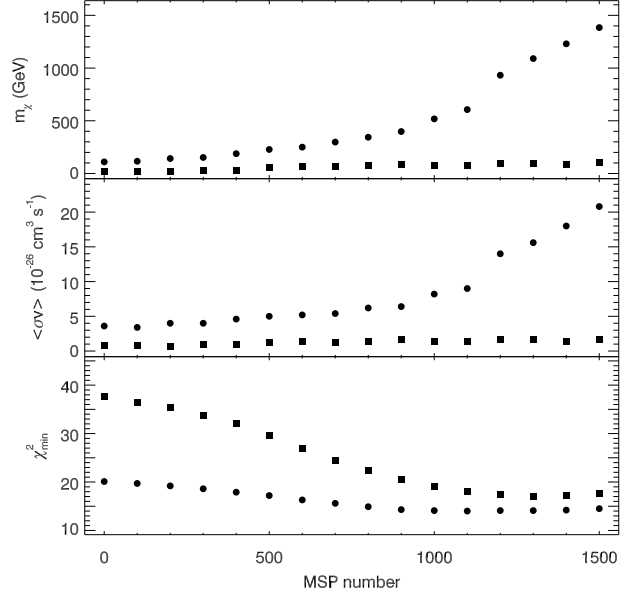


Figure 7. χ^2_{min} values resulting from different MSP numbers (bottom panel), obtained with fitting the GCE γ -ray spectrum with those of the MSPs plus DM annihilating to $b\bar{b}$ (circles) or to $\tau^+\tau^-$ (squares). The corresponding DM’s $\langle\sigma v\rangle$ and m_χ values are shown in the middle and top panel respectively.

$b\bar{b}$ model fitting. The spectral fitting results from the 1100 MSPs plus $b\bar{b}$ model is shown in the left panel of Figure 8, which had the minimum χ^2_{min} value (14.0) in the joint fitting. The 1σ – 3σ uncertainty ranges for the DM’s parameters are shown in the right panel of Figure 8.

5. DISCUSSION AND SUMMARY

We have performed a detailed study of the GCE γ -ray emission by analyzing 15 yrs of the data collected with *Fermi*-LAT. The GCE region we considered was a circular one with radius 10° . Among 25 energy bands divided from 0.3 GeV to 500 GeV, we obtained the flux measurements in 8 successive bands centered at 1–10 GeV, which likely were the more significant part of the GCE emission. The spatially resolved flux measurements were fit with a g-NFW profile, which is often considered as that for the DM distribution in the GC, and $\gamma=1.1$ was obtained. This value is the same as that obtained in Abazajian et al. (2014), but lower than the values of ~ 1.2 – 1.3 obtained in other previous studies (e.g., Hooper & Goodenough 2011; Hooper & Linden 2011; Abazajian & Kaplinghat 2012; Gordon & Macías 2013; Calore et al. 2015b,a; Daylan et al. 2016b; Di Mauro 2021). In our results, $\gamma=1.2$ was marginally disfavored in the energy band centered at 3.7 GeV at a confidence level of $\sim 2.7\sigma$ (a χ^2 value of 17.9 was obtained for 6

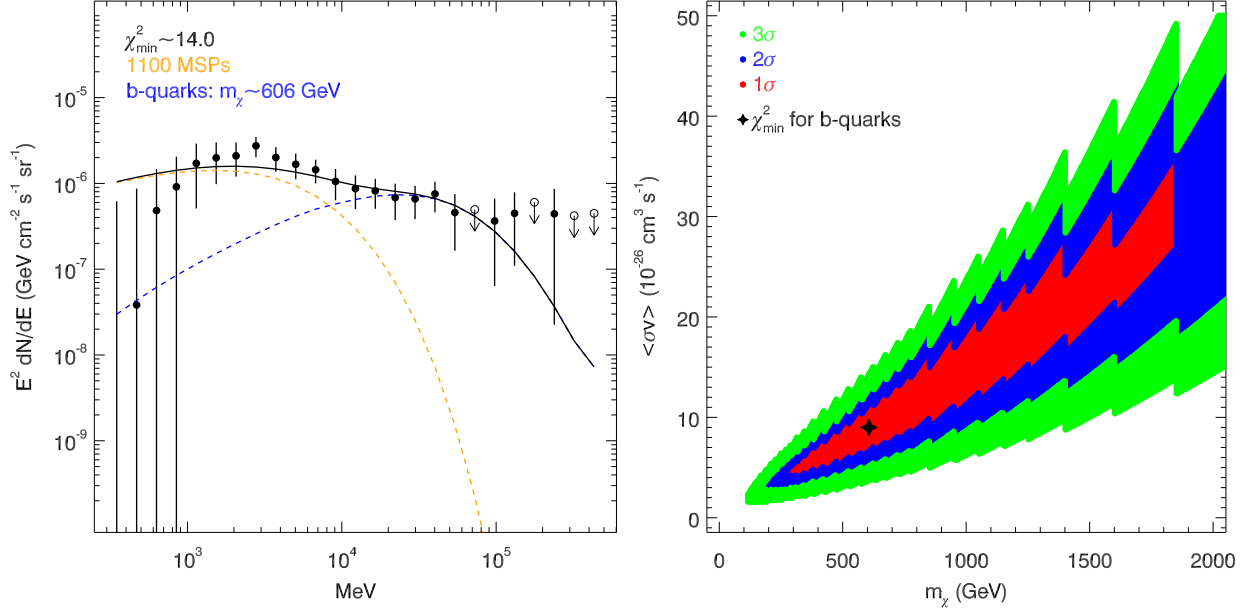


Figure 8. MSP plus the DM channel $b\bar{b}$ fitting to the γ -ray spectrum of the GCE emission. *Left:* the best fit provided by 1100 MSPs (yellow dashed line) plus the DM’s $m_\chi=606$ GeV and $\langle\sigma v\rangle = 9.0\times 10^{-26}$ $\text{cm}^3 \text{s}^{-1}$ (blue dashed line). The spectrum added from the two components is shown as a black solid line. *Right:* the 3σ uncertainty ranges for the parameters of the DM channel $b\bar{b}$, with the best-fit values marked as a black star.

DoF; see Section 3). As Di Mauro (2021) have obtained a 10% systematic uncertainty on γ , which is 1.08–1.32, our result of $\gamma=1.1$ is within the uncertainty.

Setting the g-NFW profile with $\gamma=1.1$ as a template in the source model, the γ -ray spectrum of the GCE emission was extracted. We would like to point out that this spectrum can be affected by the profile chosen to be used, but the spectral shape is less affected. We tested the g-NFW profiles with γ values of 1.0 or 1.2, as well as other spatial templates such as the Moore (Diemand et al. 2004) and the Einasto (Merritt et al. 2006; Navarro et al. 2010) profiles, and the resulting γ -ray spectra appeared higher or lower than that we obtained with $\gamma=1.1$. However our comparison indicated that the spectral shapes were consistent with each other within uncertainties.

With the obtained spectrum of the GCE emission, we tested the MSP scenario by fitting it with those constructed from different numbers of MSPs. Previously, a number of $\sim 10^3$ MSPs was suggested to constitute a reasonable source for the GCE (e.g., Abazajian & Kaplinghat 2012; Gordon & Macías 2013). Our fitting limited the number to ~ 1700 . However the MSP-model spectrum suffers the problems of having higher fluxes in the ≤ 1 GeV energy range and lower fluxes in the ≥ 10 GeV energy range comparing to the GCE’s spectrum (Figure 2). The minimum χ^2_{min} value we found was 42.4, even higher than that from the fitting with the DM channel $\tau^+\tau^-$. There are 21 spectral data

points in the GCE spectrum (not including the upper limits), and the generation of a spectrum for a number of MSPs is the Monte Carlo process have six parameters (P , τ_a , η , and Γ and E_c of a γ -ray spectrum, plus the number of MSPs). DoF in the fitting was 15, and $\chi^2_{min} = 42.4$ corresponds to a p -value of $\sim 2\times 10^{-4}$. This p -value suggests that the MSPs origin is rejected at a 3.7σ confidence level.

The high-energy tail in the spectrum of the GCE emission has been noted in previous studies such as Calore et al. (2015a) and Linden et al. (2016). Calore et al. (2015b) pointed out that the use of the P6_V11 Galactic diffuse emission model may lead to an over-subtraction of the GCE emission above ~ 10 GeV. Our analysis with the model used still indicated significant detection of the high-energy tail. One possible explanation for the tail involves the scenario that electrons produced by pulsars ICS cosmic background microwave photons to high-energy ones (Linden et al. 2016). This possibility has been used to interpret the high-energy γ -ray emission from the Sagittarius dwarf spheroidal galaxy (Crocker et al. 2022). However the ICS would be weak in an environment like the Galactic bulge because much of the energy carried by escaping electrons would be lost due to synchrotron radiation (Crocker et al. 2022). Because of the obvious discrepancy between the GCE’s and MSPs’ spectra in ≥ 10 GeV energy range, we also performed the stacking analysis of the 30–500 GeV data of 96 γ -ray MSPs for possibly

resolving the discrepancy by checking if MSPs would have significant high-energy emission. Only upper limits were obtained, and the scaled values for 1661 MSPs were lower than the spectral data points of the GCE. Thus both the fitting results and the obvious discrepancy in the high energy range suggest that MSPs alone are not likely the source of the GCE emission.

We considered the DM annihilation models for the GCE emission for comparison, and found that the channel $b\bar{b}$ with $m_\chi=110$ GeV and $\langle\sigma v\rangle=3.6\times 10^{-26}$ cm³ s⁻¹ could provide the best fit. The χ^2_{min} value was 20.1, corresponding to a p -value of 0.4 (for 19 DoF). The m_χ value is higher than that obtained in previous studies (several tens of GeV, e.g., Hooper & Goodenough 2011; Abazajian & Kaplinghat 2012; Calore et al. 2015b,a; Daylan et al. 2016a; Huang et al. 2016; Di Mauro 2021). We note that Calore et al. (2015a) found a maximum m_χ of ~ 74 GeV at a p -value of >0.05 in the case of the channel $b\bar{b}$, which is within the uncertainty ranges we obtained (see the right panel of Figure 2). In Figure 2, a model spectrum with $m_\chi=50$ GeV ($\langle\sigma v\rangle=1.8\times 10^{-26}$ cm³ s⁻¹; see Calore et al. 2015a,b) is shown as a comparison example. As can be seen, this spectrum is very similar to our MSP model spectrum and can not provide any fits to the high-energy part of the GCE's spectrum (the fitting gives $\chi^2_{min}=33.8$). There are differences between our analysis and previous ones that should be noted: more LAT data and the latest source catalog were used in our analysis.

In order to fit the whole spectrum of the GCE emission as much as possible, the combination of the channels $b\bar{b}$ and $\tau^+\tau^-$ was tested. The best fit had $\chi^2_{min}=12.4$, corresponding to a p -value of 0.8 (for 18 DoF). The branching ratio into $b\bar{b}$ was 0.7 for this case, and the corresponding m_χ and $\langle\sigma v\rangle$ were 68 GeV and 2.8×10^{-26} cm³ s⁻¹ respectively. The m_χ value is close to that obtained in the previously studies. We applied the F -test to evaluation of the significance of an additional annihilation channel (Protassov et al. 2002). For an additional channel $b\bar{b}$ to the only channel $\tau^+\tau^-$, the F -test probability of finding a fit improvement by chance is 1×10^{-5} , which corresponds to a significance of 4.4σ . For an additional channel $\tau^+\tau^-$ to the only channel $b\bar{b}$, the F -test probability is 4×10^{-3} , which corresponds to a significance of 2.8σ .

We also explored the case that both MSPs and DM annihilations contribute to the GCE emission. Given the low-energy cutoff in the γ -ray spectra of MSPs, the DM annihilation is thus needed for the high-energy part of the GCE emission. Varying MSP number, the best-fit we obtained was when there were 1100 MSPs plus the channel $b\bar{b}$ with $m_\chi \simeq 600$ GeV and $\langle\sigma v\rangle =$

9.0×10^{-26} cm³ s⁻¹ ($\chi^2_{min}=14.0$). We note that in the joint model fitting, the DM's m_χ and $\langle\sigma v\rangle$ were obtained with large uncertainties (see the right panel of Figure 8), which is likely due to the large uncertainties of the spectral data points in the high energy range (i.e., can not provide strong constraints in the fitting). While the MSPs essentially provide the low-energy part for the GCE emission in the joint fitting, there has also been the pure DM annihilation scenario suggested to be able to provide a fit. In this scenario, a two-component DM model is required (e.g., Linden et al. 2011; Abazajian et al. 2015): the low-energy emission would arise from ICS of the electrons produced from the annihilations of light DM particles.

We estimate the fit improvement from the joint model to check if the MSPs are needed. As in the fitting, the model spectrum of a given number of MSPs was obtained by averaging 1000 spectra, with each resulting from a run, the number of MSPs was the only additional parameter in addition to the two parameters from the DM annihilations. Applying the F -test to the case of the MSPs plus the DM channel $b\bar{b}$ comparing to the pure DM channel $b\bar{b}$, the probability of finding a fit improvement by chance is ~ 0.01 , corresponding to a confidence level of $\sim 2.5\sigma$. Thus an additional MSP component is only marginally needed for the GCE emission.

We summarize our results as follows:

1. A g-NFW profile with γ of 1.1 is found to describe the γ -ray morphology of the GCE.
2. Fitting the obtained spectrum of the GCE emission, ~ 1700 MSPs are found to be needed, while the MSP model spectrum can not provide any fits for the ≥ 10 GeV part of the spectrum.
3. Stacking analysis is performed for 96 nearby γ -ray MSPs, but no significant emission in 30–500 GeV energy range is detected, which verifies the mismatch between the spectra of the GCE emission and the MSPs in the ≥ 10 GeV high-energy range.
4. DM annihilation channels $\tau^+\tau^-$ and $b\bar{b}$ are tested for fitting the GCE's spectrum. The latter provide a better fit than the former (with p -values of 0.4 and 6×10^{-3} respectively). The best-fit m_χ and $\langle\sigma v\rangle$ values of the DM $b\bar{b}$ model are 110 GeV and 3.6×10^{-26} cm³ s⁻¹, respectively. When combining the two channels, 70% $b\bar{b}$ plus 30% $\tau^+\tau^-$ provides the best fit.
5. For the case of having contributions from both MSPs and DM annihilations, the MSPs plus the $b\bar{b}$ model always provides better fits than the MSPs

plus the $\tau^+\tau^-$ model. Comparing the former to the pure DM $b\bar{b}$ model, the MSP component is found to be marginally needed.

This research is supported by the Original Innovation Program of the Chinese Academy of Sciences (E085021002). Z.W. acknowledges the support by the Basic Research Program of Yunnan Province (No. 202201AS070005) and the National Natural Science Foundation of China (12273033).

REFERENCES

- Abazajian, K. N., Canac, N., Horiuchi, S., & Kaplinghat, M. 2014, *PhRvD*, 90, 023526
- Abazajian, K. N., Canac, N., Horiuchi, S., Kaplinghat, M., & Kwa, A. 2015, *JCAP*, 2015, 013
- Abazajian, K. N., Horiuchi, S., Kaplinghat, M., Keeley, R. E., & Macias, O. 2020, *PhRvD*, 102, 043012
- Abazajian, K. N., & Kaplinghat, M. 2012, *PhRvD*, 86, 083511
- Abbate, F., Mastrobuono-Battisti, A., Colpi, M., et al. 2018, *MNRAS*, 473, 927
- Abdo, A. A., Ackermann, M., Ajello, M., et al. 2009, *ApJL*, 706, L1
- . 2010, *ApJ*, 718, 348
- Abdollahi, S., Acero, F., Ackermann, M., et al. 2020, *ApJS*, 247, 33
- Ackermann, M., Ajello, M., Atwood, W. B., et al. 2012, *ApJ*, 750, 3
- Ackermann, M., Ajello, M., Albert, A., et al. 2017a, *ApJ*, 840, 43
- . 2017b, *ApJ*, 840, 43
- Arcadi, G., Dutra, M., Ghosh, P., et al. 2018, *European Physical Journal C*, 78, 203
- Atwood, W. B., Abdo, A. A., Ackermann, M., et al. 2009, *ApJ*, 697, 1071
- Ballet, J., Bruel, P., Burnett, T. H., Lott, B., & The Fermi-LAT collaboration. 2023, *arXiv e-prints*, [arXiv:2307.12546](https://arxiv.org/abs/2307.12546)
- Bartels, R., Krishnamurthy, S., & Weniger, C. 2016, *PhRvL*, 116, 051102
- Bertone, G., Hooper, D., & Silk, J. 2005, *PhR*, 405, 279
- Brandt, T. D., & Kocsis, B. 2015, *ApJ*, 812, 15
- Calore, F., Cholis, I., McCabe, C., & Weniger, C. 2015a, *PhRvD*, 91, 063003
- Calore, F., Cholis, I., & Weniger, C. 2015b, *JCAP*, 2015, 038
- Cirelli, M., Corcella, G., Hektor, A., et al. 2011, *JCAP*, 2011, 051
- Crocker, R. M., Macias, O., Mackey, D., et al. 2022, *Nature Astronomy*, 6, 1317
- Daylan, T., Finkbeiner, D. P., Hooper, D., et al. 2016a, *Physics of the Dark Universe*, 12, 1
- . 2016b, *Physics of the Dark Universe*, 12, 1
- Di Mauro, M. 2021, *PhRvD*, 103, 063029
- Diemand, J., Moore, B., & Stadel, J. 2004, *MNRAS*, 353, 624
- Fragione, G., Antonini, F., & Gnedin, O. Y. 2018, *MNRAS*, 475, 5313
- Funk, S. 2015, *Proceedings of the National Academy of Science*, 112, 12264
- Gordon, C., & Macias, O. 2013, *PhRvD*, 88, 083521
- H. E. S. S. Collaboration, Aharonian, F., Ait Benkhali, F., et al. 2023, *Nature Astronomy*, [arXiv:2310.06181](https://arxiv.org/abs/2310.06181)
- Hooper, D., & Goodenough, L. 2011, *Physics Letters B*, 697, 412
- Hooper, D., & Linden, T. 2011, *PhRvD*, 84, 123005
- Hooper, D., & Mohlabeng, G. 2016, *JCAP*, 2016, 049
- Hooper, D., & Slatyer, T. R. 2013, *Physics of the Dark Universe*, 2, 118
- Huang, X., Enßlin, T., & Selig, M. 2016, *JCAP*, 2016, 030
- Huber, B., Farnier, C., Manalaysay, A., Straumann, U., & Walter, R. 2012, *A&A*, 547, A102
- Iocco, F., Pato, M., Bertone, G., & Jetzer, P. 2011, *JCAP*, 2011, 029
- Linden, T., Hooper, D., & Yusef-Zadeh, F. 2011, *ApJ*, 741, 95
- Linden, T., Rodd, N. L., Safdi, B. R., & Slatyer, T. R. 2016, *PhRvD*, 94, 103013
- Macias, O., Gordon, C., Crocker, R. M., et al. 2018, *Nature Astronomy*, 2, 387
- Manchester, R. N., Hobbs, G. B., Teoh, A., & Hobbs, M. 2005, *AJ*, 129, 1993
- Merritt, D., Graham, A. W., Moore, B., Diemand, J., & Terzić, B. 2006, *The Astronomical Journal*, 132, 2685
- Navarro, J. F., Frenk, C. S., & White, S. D. M. 1996, *ApJ*, 462, 563
- . 1997, *ApJ*, 490, 493
- Navarro, J. F., Ludlow, A., Springel, V., et al. 2010, *MNRAS*, 402, 21

- Protassov, R., van Dyk, D. A., Connors, A., Kashyap, V. L., & Siemiginowska, A. 2002, *ApJ*, 571, 545
- Smith, D. A., Bruel, P., Clark, C. J., et al. 2023, arXiv e-prints, arXiv:2307.11132
- Springel, V., White, S. D. M., Frenk, C. S., et al. 2008, *Nature*, 456, 73
- Su, M., Slatyer, T. R., & Finkbeiner, D. P. 2010, *ApJ*, 724, 1044
- Vanhollebeke, E., Groenewegen, M. A. T., & Girardi, L. 2009, *A&A*, 498, 95
- Wu, W., Wang, Z., Xing, Y., & Zhang, P. 2022, *ApJ*, 927, 117
- Xing, Y., & Wang, Z. 2016, *ApJ*, 831, 143
- Zhang, P., Xing, Y., & Wang, Z. 2022, *ApJL*, 935, L36
- Zhang, P., Xing, Y., Wang, Z., Wu, W., & Chen, Z. 2023, *ApJ*, 945, 70
- Zhou, B., Liang, Y.-F., Huang, X., et al. 2015, *PhRvD*, 91, 123010

Table 1. Spectral fitting results for the GCE emission

Spectral Model	χ^2_{min}	MSP number	DM m_χ (GeV)	DM $\langle\sigma v\rangle$ ($10^{-26} \text{ cm}^3 \text{ s}^{-1}$)	p -value
MSP	42.4	1661 (1415–1706)	2×10^{-4}
DM $b\bar{b}$	20.1	...	110	3.6	0.4
DM $\tau^+\tau^-$	37.6	...	16	0.8	6×10^{-3}
DM $b\bar{b} + \tau^+\tau^-$	12.4	...	68	2.8	0.8
MSP + DM $b\bar{b}$	14.0	1100	606	9.0	0.7
MSP + DM $\tau^+\tau^-$	17.1	1300	94	1.6	0.5

Table 2. Stacking analysis results for 96 γ -ray MSPs

Band (GeV)	$F^{up}/10^{-11}$ (GeV cm $^{-2}$ s $^{-1}$)	TS	$F_s^{up}/10^{-8}$ (GeV cm $^{-2}$ s $^{-1}$ sr $^{-1}$)
30.0–76.6	3.34	14	1.83
76.6–195.7	0.39	0	0.21
195.7–500.0	1.85	0	1.01

Note: F^{up} is the energy flux ($E^2 dN/dE$) upper limit obtained from the stacking analysis. F_s^{up} is the upper limit scaled for 1661 MSPs in the GCE region.